10.1071/WF14023_AC

Supplementary Material: *International Journal of Wildland Fire*, 2015, 24, 14-26.

Supplementary Material

Correlations between components of the water balance and burned area reveal new insights for predicting forest-fire area in the southwest United States

A. Park Williams[A,I], *Richard Seager*[A], *Alison K. Macalady*[B], *Max Berkelhammer*[C], *Michael A. Crimmins*[D], *Thomas W. Swetnam*[B], *Anna T. Trugman*[E], *Nikolaus Buenning*[F], *David Noone*[C], *Nate G. McDowell*[G], *Natalia Hryniw*[H], *Claudia I. Mora*[G] *and Thom Rahn*[G]

[A]Lamont-Doherty Earth Observatory of Columbia University, Palisades, NY 10964, USA.

[C]Laboratory of Tree-Ring Research, University of Arizona, Tucson, AZ 85724, USA.

[D]Department of Atmospheric & Oceanic Sciences, Cooperative Institute for Research in Environmental Sciences, University of Colorado, Boulder, CO 80309, USA.

[E]Department of Atmospheric & Oceanic Sciences, Princeton University, Princeton, NJ 08544, USA.

[F]Department of Earth Sciences, University of Southern California, Los Angeles, CA 90089, USA.

[G]Earth & Environmental Sciences Division, Los Alamos National Laboratory, Los Alamos, NM 87545, USA.

[H]Department of Atmospheric Sciences, University of Washington, Seattle, WA 98195, USA.

[I]Corresponding author. Email: williams@ldeo.columbia.edu

S1. Use of MODIS to estimate burned area in 2013

The Moderate Resolution Imaging Spectroradiometer (MODIS) burned-area product (version 5.1) (Roy *et al.* 2008) has 500 m geographic resolution, begins in 2000 and classifies burned areas in terms of confidence (four confidence classes) rather than severity. In forest, we considered all MODIS burned areas regardless of confidence because the 'all-confidence' MODIS record generally agrees best with the MTBS record of moderate and severe burned areas during the overlapping period. For non-forest area, we only considered the highest-confidence MODIS burned areas to maximise agreement with MTBS. We adjusted the 2013 MODIS-derived values based on linear relationships between MTBS and MODIS during the overlapping 2000–2012 period. MODIS and MTBS burned-area time series are shown in Figure S1.

10.1071/WF14023_AC

Supplementary Material: *International Journal of Wildland Fire*, 2014, 23

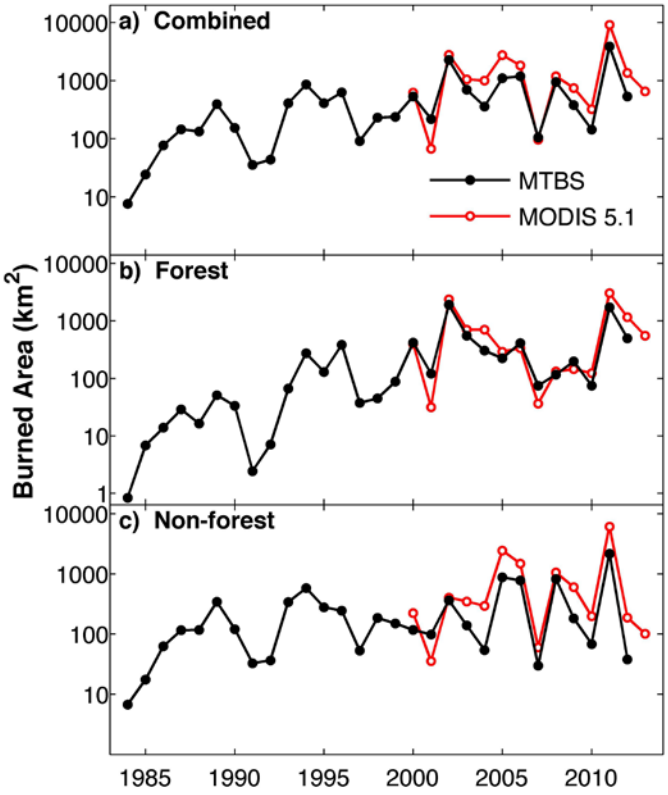

Fig. S1. Time series of MTBS (1984–2012) and MODIS 5.1 (2000–2013) annual burned area.

S2. Use of PRISM to monitor regional climate variability in the SW

It is worthwhile to compare PRISM climate records (Daly *et al.* 2004) to records derived from alternate datasets because PRISM data, and other datasets, may contain artifacts, particularly in long-term trends, due to the ever-changing network of climate stations that feed into the dataset (e.g., Hamlet and Lettenmaier 2005). In Figure S2 we compare records of PRISM climate anomalies for the southwest United States (SW) region against a suite of records derived from alternate datasets. Strong agreement among datasets in panels A and B indicates that the methodological qualities unique to development of the PRISM dataset do not make PRISM records of temperature and precipitation in the SW (at least during the range of months focused on in our study) less reliable than other available products in terms of regional trends and interannual variability.

10.1071/WF14023_AC

Supplementary Material: *International Journal of Wildland Fire*, 2014, 23

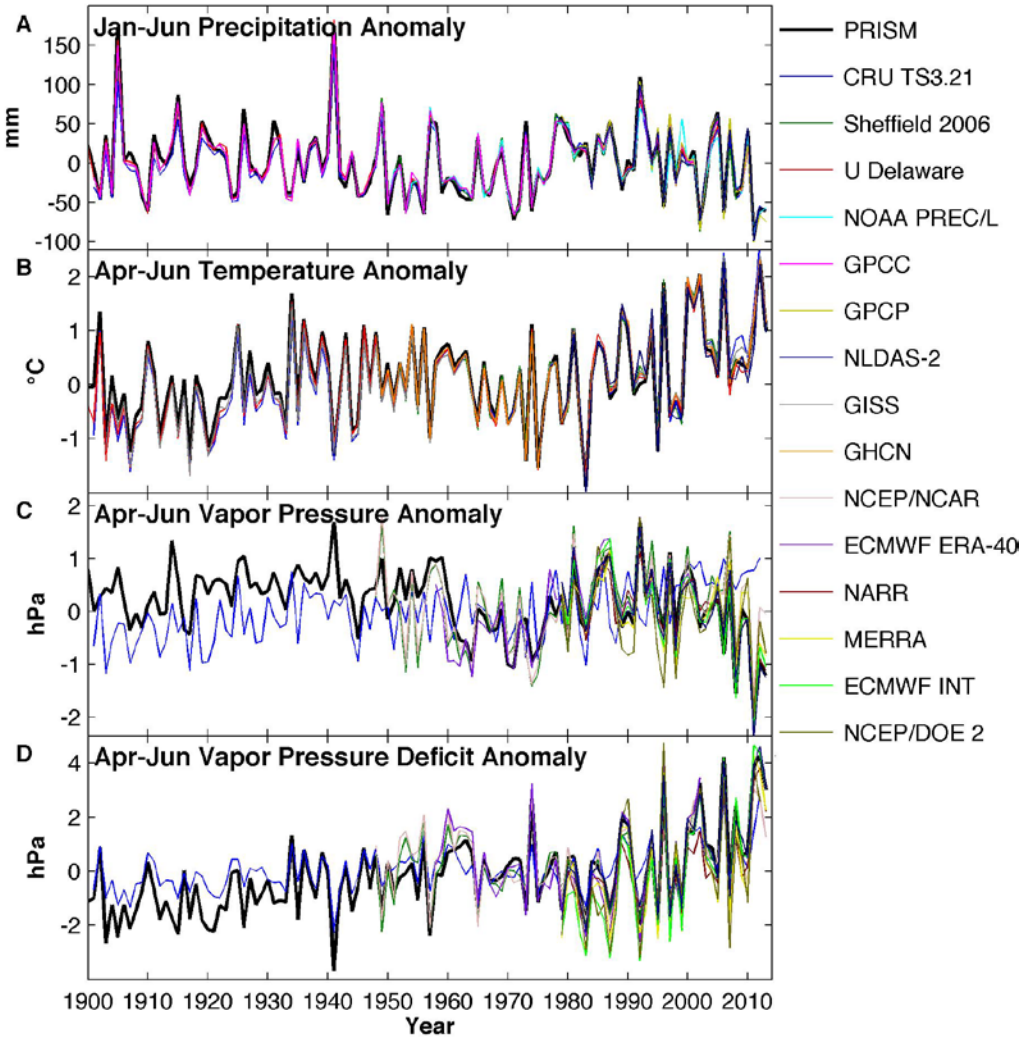

Fig. S2. Comparison of PRISM records of SW climate to alternate datasets. Anomalies are calculated relative to the 1961–1999 mean. Records beginning in 1979 were adjusted to have the same mean anomaly as PRISM during overlapping years.

Strong agreement among various records of regional temperature and precipitation is not surprising because measurements of these variables have been collected at a relatively high density of locations throughout the period of record. This is not the case, however, for atmospheric humidity (often recorded as dew point). The network of stations from which PRISM dew-point estimates are derived is relatively sparse (Daly *et al.* 2004) and has undergone a large increase in density in recent decades. Despite these known problems, Figure S2C indicates general agreement among various representations of vapour-pressure variability in the SW since the 1970s. With the exception of the CRU TS3.21 record, which does not agree with any of the alternate records of vapour pressure, the alternate records agree upon an increase in SW April–June dew point from the early 1960s (though most alternate records begin in 1979) through late 1980s, followed by a decline from the early 1990s through present.

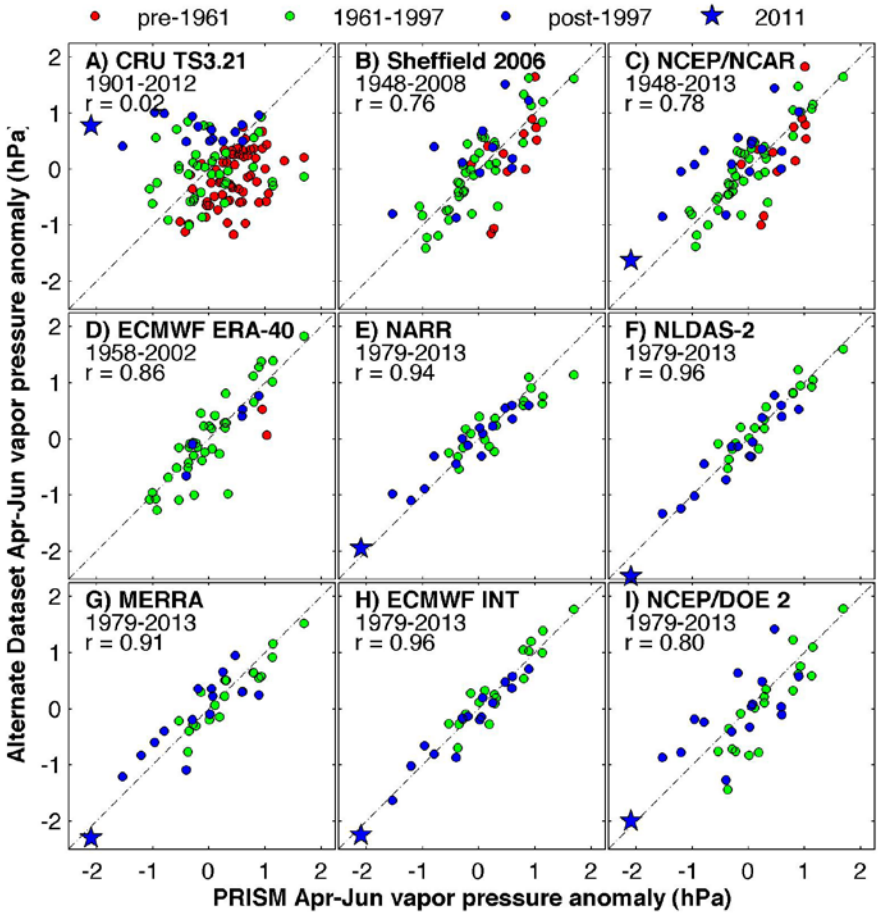

Fig. S3. Regression plots of annual April–June vapour pressure anomalies calculated with 8 alternate datasets versus PRISM anomalies. Different colours represent periods when different methodologies in the PRISM vapour-pressure calculation may be suspected of causing artificial inhomogeneity in the PRISM time series.

PRISM dew-point data prior to 1961 are estimated based on empirical relationships with daily temperature range and precipitation (C. Daly, per. comm.). This shift in methodology may introduce artificial mid-century trends in dew point that are difficult to identify because of a lack of validation data. Indeed, the PRISM record in Figure S2C contains a step-wise downward shift in the early 1960s that is not shared among the alternate re-analysis datasets). The pre-1961 difference between PRISM and the alternate datasets may be more easily observed in Figure S3A–D, where PRISM indicates higher pre-1961 humidity anomalies than the alternate datasets, but post-1961 anomalies agree well with the alternate datasets. Notably, the stepwise downward shift in PRISM dew point at 1961 (whether it is accurate or not) does not influence our regressions of climate versus burned-area data because the burned-area data do not begin until 1984. Additionally, we base all calculations of climate anomalies relative to 1961–2013 because it is probable that no dataset accurately captures SW humidity variability prior to 1961, when observation density was relatively sparse. Following 1961, agreement among humidity records is much better, particularly during 1979 to present (Fig. S3E–I).

Notably, variability among humidity records does not contribute much toward uncertainty in VPD (Fig. S2D). Relatively strong agreement among VPD records despite some spread among humidity records demonstrates the dominant role of temperature in dictating VPD

variability in the SW, though there are exceptional years such as 2011 when humidity plays a critical role in dictating VPD anomalies.

In addition to the 1961 shift in dew-point methodology, the PRISM methodology changed following 1997, when PRISM began producing datasets in real time (Di Luzio *et al.* 2008). Also, the network of vapour-pressure readings that PRISM uses increased in density dramatically during the late 1990s and early 2000s due to increased data coming from networks of remote weather stations such as the Remote Automated Weather Stations (RAWS) network (as well as AgriMet, ASOS, COOP and WBAN) (C. Daly, pers. comm.). In Figure S3 we show that there is no consistent shift in how PRISM vapour-pressure records relate to the alternate records over the past couple of decades. Additionally, the five non-CRU vapour-pressure records that include data for 2011 agree with PRISM that 2011 April–June vapour pressure was by far the lowest on record. Among the five datasets, the average 2011 vapour-pressure anomaly represented a 29% reduction from the 1961–1999 mean, compared to a 30% reduction according to PRISM.

S3 Calculation of monthly VPD

VPD was calculated as saturation vapour pressure (e_s) minus actual vapour pressure (e). Temperature dictates e_s and humidity dictates e. We estimated average monthly temperature (T_{ave}) as a mixture of monthly means of daily maximum temperature (T_{max}) and daily minimum temperature (T_{min}). The relative contributions of T_{max} and T_{min} were derived for each month from hourly gridded (0.125° geographic resolution) temperature data from the 1979–2013 North American Land Data Assimilation System project phase 2 (NLDAS-2, Mitchell *et al.* 2004), where the contribution of T_{max} toward T_{ave} ranges from 43.1% in December to 52.8% in June. To calculate VPD, we calculated e_s and e by substituting T_{ave} and dew point, respectively, for T in the following equation:

$$e_s = 6.1121 \exp[17.502 * T / (240.97 + T)] \quad \text{(eqn S1)}$$

where units of T and e are °C and hPa, respectively (Kunkel 2001). We then calculated VPD ($e_s - e$).

We adjusted the VPD values to account for a systematic and linear underestimation that occurs when monthly mean VPD is calculated from monthly mean T_{ave} and dew point. Due to the exponential influence of temperature on saturation vapour pressure, averaging temperature and dew point data over time before calculating VPD causes calculated VPD to be artificially low. To evaluate this bias, we utilised hourly re-analysis data from the North American Land Data Assimilation System project phase 2 (NLDAS-2, Mitchell *et al.* 2004) for 1979–2013. Figure S4 shows how monthly mean VPD estimated from monthly mean T_{max}, T_{min}, and dew point data (*y-axis*) compares to monthly mean VPD calculate directly from hourly data (*x-axis*). The vertical offset of the regression line from the 1 : 1 line indicates a negative bias in monthly values estimated from monthly mean data of approximately 3.1%.

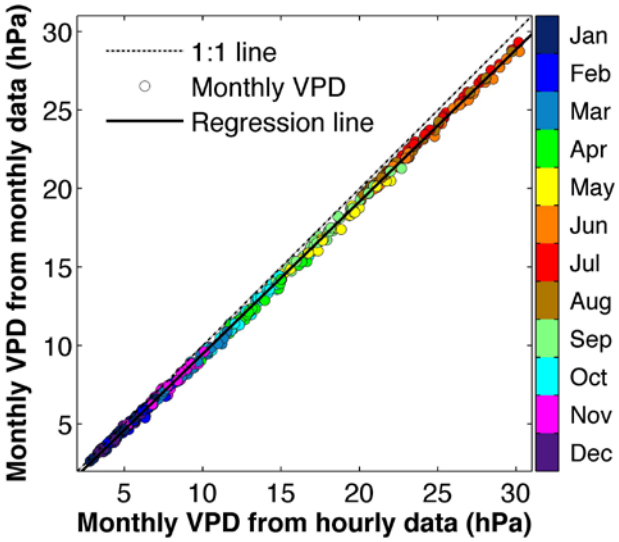

Fig. S4. Regression plot of monthly VPD values (1979–2013) for the SW calculated from monthly mean (*y-axis*) versus hourly (*x-axis*) temperature and humidity data (source: NLDAS-2).

Figure S4 indicates that the negative bias is linear with a consistent slope across months. From this set of 420 monthly samples, we derived the relationship to be:

$$\text{VPD} = 0.2415 + 1.0310(VPD_m) \quad \text{(eqn S2)}$$

where VPD_m is too low because it was calculated from monthly mean temperature and dew-point data. We used this equation to correct all monthly mean VPD values calculated from PRISM data.

The CMIP5 data archive does not include projections of VPD. We calculated e from projected specific humidity (q) and surface pressure (P):

$$e = P\,[\,M_{dry} / [M_{wet}\,(1/q - 1) + M_{dry}\,]] \quad \text{(eqn S3)}$$

where P is in units of hPa, q is in units of kg water vapour per kg air, and M_{dry} and M_{wet} are molar masses of dry and wet air, respectively (M_{dry} = 28.9644 g mol^{-1}, M_{wet} = 18.01534 g mol^{-1}) (derived from Lowe and Ficke (1974)). We calculated e_s using equation S1 and adjusted monthly VPD values using equation S2.

S4. NLDAS-2 data

NLDAS-2 near-surface (10 m) hourly wind data are based on the three-hourly National Center for Environmental Prediction (NCEP) North America Regional Reanalysis (NARR), produced by assimilating surface measurements and radiosonde data into atmospheric simulations (Mesinger *et al.* 2006). NLDAS-2 downward shortwave radiation are also based on NARR, but bias corrected to the University of Maryland Surface Radiation Budget dataset (Pinker *et al.* 2003), which was developed using GOES-8 satellite data. For soil moisture, potential evapotranspiration (PET) and evapotranspiration, we used simulation output from the Noah land-surface model, which is forced by NLDAS-2 data (Xia *et al.* 2012). PET is calculated within the Noah model using a modified version of the Penman–Monteith formulation (Penman 1948) that integrates meteorological data and satellite-derived estimates of land-cover characteristics into the land-surface model (Mahrt and Ek 1984; Chen and Dudhia 2001).

S5. Increasing annual area, size, frequency and elevation range of forest fires

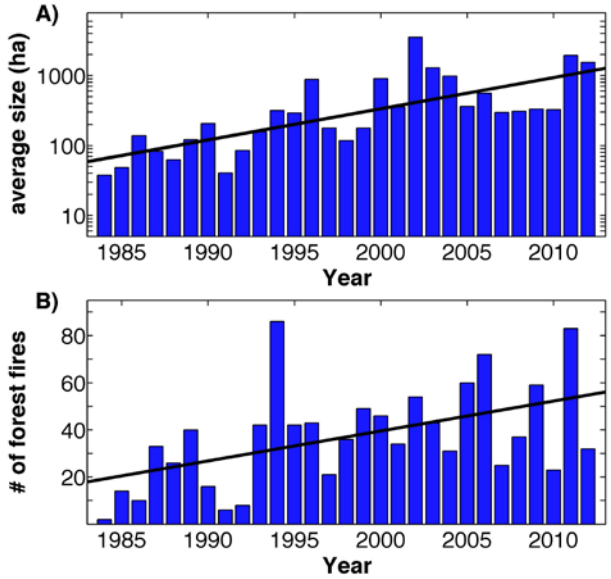

Fig. S5. Annual average size (A) and number (B) of forest fires for 1984–2012. These values were calculated from MTBS data (because the MODIS burned-area product does not explicitly include information on individual wildfires). As in our other analyses here, we only include moderate and severe burned areas within forest.

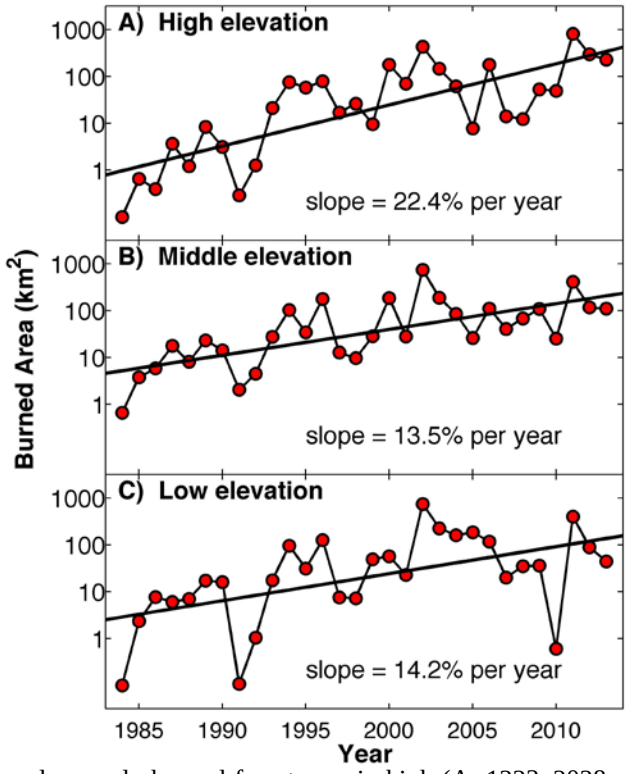

Fig. S6. Annual moderately and severely burned forest area in high (A: 1223–2028 m), middle (B: 2029–2431 m) and low (C: 2432–3656 m) elevations. Elevations represent the upper (A), middle (B) and lower terciles of forested elevations burned moderately and severely during 1984–2013.

S6. Alternate calculations of correlation between climate and burned area

10.1071/WF14023_AC

Supplementary Material: *International Journal of Wildland Fire*, 2014, 23

Table S1. Spearman rank correlation between log_{10} annual 1984–2013 SW burned area (moderate and severe) and seasonal climate during the period of 3–6 consecutive months when correlation is optimised

All 3–6 month periods were considered within the 24-month window that begins in January of the prior year and ends in December of the current year. First-order autocorrelation was not removed from climate or burned-area records. Instead, all time series were ranked from lowest to highest and correlations were calculated for the time series of rank values. Subscript 'p' following a month indicates the prior year

	All SW		Forest		Non-forest	
	Months	**r**	**Months**	**r**	**Months**	**r**
VPD	Apr–Jul	0.77	May–Aug	0.86	Jan_p–May_p	–0.50
log_{10}(precipitation)	Mar–Jul	–0.77	Mar–Aug	–0.75	Jan_p–May_p	0.64
T_{max}	Apr–Aug	0.68	Jun–Aug	0.74	Dec_p–Feb	0.49
es	Jun–Aug	0.70	Jun–Aug	0.78	Jun –Aug	0.44
e	Apr–Jul	–0.69	Apr–Jul	–0.59	Mar_p–Aug_p	0.54
Relative humidity	Apr–Jul	–0.76	May–Jul	–0.77	Jan_p–May_p	0.50
PET	Apr–Jul	0.78	Mar–Jul	0.81	Jun–Nov	0.53
Water deficit	Mar–Jul	0.79	Apr–Aug	0.83	Apr–Jul	0.50
Insolation	Apr–Jul	0.76	May–Jul	0.67	Apr–Jul	0.50
Wind speed	Jan–Mar	0.68	Jan–Apr	0.68	Jun–Aug	0.58
Soil moisture	Mar–Aug	–0.76	Apr–Aug	–0.83	Feb_p–Apr_p	0.54
KBDI	Jun–Aug	0.65	May–Oct	0.80	Apr_p–Jul_p	–0.46
PDSI	Jun–Aug	–0.66	Feb–Apr	–0.82	Oct–Dec	–0.36
SPEI	Mar–Aug	–0.70	Mar–Aug	–0.71	Apr–Sep	–0.52
ERC	Apr–Aug	0.78	May–Aug	0.82	Feb_p–May_p	–0.53

Table S2. Pearson's correlation between log_{10} annual 1984–2013 SW burned area (moderate and severe) and seasonal climate during the period of 3–6 consecutive months when correlation is optimised

All 3–6 month periods were considered within the 24-month window that begins in January of the prior year and ends in December of the current year. Time series were not adjusted prior to correlation analysis. Subscript 'p' following a month indicates the prior year

	All SW		Forest		Non-forest	
	Months	**r**	**Months**	**r**	**Months**	**r**
VPD	Jun–Aug	0.74	Jun–Aug	0.80	Jun–Aug	0.52
log_{10}(precipitation)	Mar–Jul	–0.72	Mar–Aug	–0.69	Mar–Jul	–0.61
T_{max}	Jun–Aug	0.69	Jun–Aug	0.73	Jun–Aug	0.53
es	Jun–Aug	0.70	Jun–Aug	0.76	Jun–Aug	0.50
e	Apr–Aug	–0.63	Apr–Jul	–0.57	Apr–Jul	–0.53
Relative humidity	Apr–Aug	–0.70	May–Aug	–0.72	Apr–Jul	–0.52
PET	Apr–Jul	0.75	Mar–Aug	0.77	Apr–Jul	0.54

Water deficit	Apr–Aug	0.74	Mar–Aug	0.79	Apr–Jul	0.55
Insolation	May–Jul	0.73	Mar–Jul	0.65	Apr–Jul	0.54
Wind speed	Feb–Jul	0.62	Jan–Apr	0.61	May–Aug	0.54
Soil moisture	Apr–Aug	–0.71	Mar–Aug	–0.78	Apr–Jul	–0.51
KBDI	Jun–Aug	0.62	Jun–Sep	0.73	May_p–Jul_p	–0.43
PDSI	Jul–Dec	–0.67	Jul–Dec	–0.75	Oct–Dec	–0.39
SPEI	Mar–Aug	–0.62	May–Aug	–0.60	Jun–Nov	–0.48
ERC	Jun–Aug	0.71	May–Aug	0.73	Jun–Aug	0.50

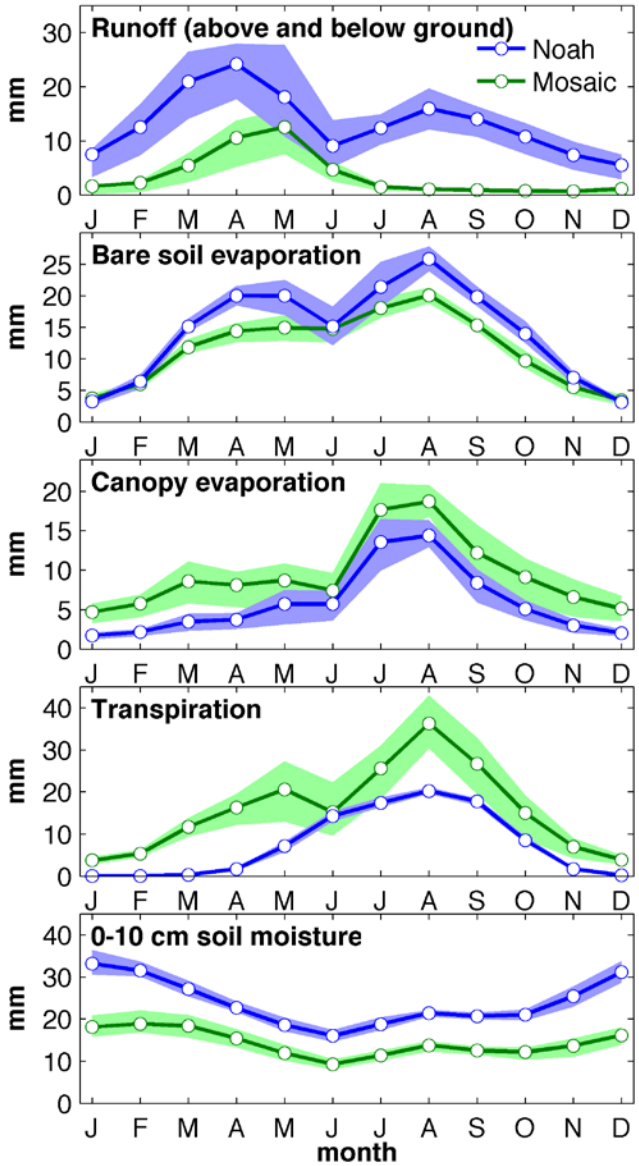

Fig. S7. Annual cycles of runoff, bare-soil evaporation, canopy evaporation, transpiration and near-surface soil moisture produced by the (blue) Noah (Chen *et al.* 1996) and (green) Mosaic (Koster and Suarez 1994) land-surface models, forced with identical NLDAS-2 meteorological data (Xia *et al.* 2012). Lines and circles represent monthly values averaged across 1979–2013. Shaded areas bound the inner quartiles to provide a sense for interannual variability.

10.1071/WF14023_AC

Supplementary Material: *International Journal of Wildland Fire*, 2014, 23

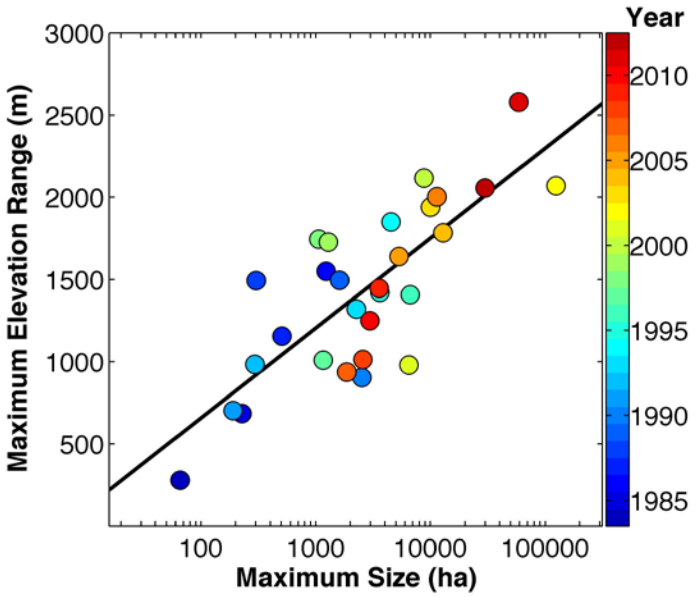

Fig. S8. Annual maximum elevation range of a forest fire (*y-axis*) versus annual size of the largest forest fire (*x-axis*) in the SW for 1984–2012. These values were calculated from MTBS data and only include moderate and severe burned areas within forest. Dot colour represents year, corresponding with the colour bar.

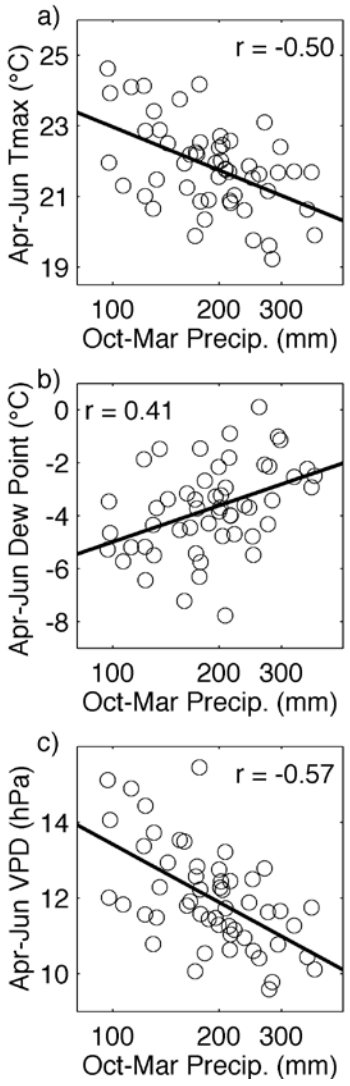

Fig. S9. Scatter plots of April–June T_{max} (a), dew point (b) and VPD (c) versus October–March precipitation total. Data represent the SW forest region, calculated from PRISM during 1961–2013. Correlations are significant ($p < 0.05$) after first order autocorrelation has been accounted for.

References

Chen F, Mitchell K, Schaake J, Xue Y, Pan H-L, Koren V, Duan QY, Ek M, Betts A (1996) Modeling of land surface evaporation by four schemes and comparison with FIFE observations. *Journal of Geophysical Research* **101**, 7251–7268.

Chen F, Dudhia J (2001) Coupling an advanced land surface-hydrology model with the Penn State-NCAR MM5 modeling system. Part 1: Model implementation and sensitivity. *Monthly Weather Review* **129**, 569–585.

Daly C, Gibson WP, Dogget M, Smith J, Taylor G (2004) Up-to-date monthly climate maps for the coterminous United States. In 'Proceedings of the 14th AMS Conference on Applied Climatology, 84th AMS Annual Meeting', 13–16 January 2004, Seattle, WA (American Meteorological Society: Boston, MA). Available from

https://ams.confex.com/ams/pdfpapers/71444.pdf?origin=publication_detail [Verified 9 October 2014]

Di Luzio M, Johnson GL, Daly C, Eischeid JK, Arnold JG (2008) Constructing retrospective gridded daily precipitation and temperature datasets for the conterminous United States. *Journal of Applied Meteorology* **47**, 475–497.

Hamlet AF, Lettenmaier DP (2005) Production of Temporally consistent gridded precipitation and temperature fields for the continental United States. *Journal of Hydrometeorology* **6**, 330–336.

Koster RD, Suarez MJ (1994) The components of a 'SVAT' scheme and their effects on a GCM's hydrological cycle. *Advances in Water Resources* **17**, 61–78.

Kunkel KE (2001) Surface energy budget and fuel moisture. In 'Forest fires: behavior and ecological effects'. (Eds Johnson EA Miyanishi K) pp. 303–350. (Academic Press: San Diego, CA)

Lowe PR, Ficke JM (1974) The computation of saturation vapor pressure. In *Technical Paper No.4-74* (Monterey, CA), p. 27.

Mahrt L, Ek MB (1984) The influence of atmosperic stability on potential evaporation. *Journal of Applied Meteorology* **23**, 222–234.

Mesinger F, DiMego G, Kalnay E, Mitchell K, Shafran PC, Ebisuzaki W, Jovic D, Woollen J, Rogers E, Berbery EH (2006) North American regional reanalysis. *Bulletin of the American Meteorological Society* **87**, 343–360.

Mitchell KE, Lohmann D, Houser PR, Wood EF, Schaake JC, Robock A, Cosgrove BA, Sheffield J, Duan Q, LLuo L, Higgins RW, Pinker RT, Tarpley JD, Lettenmaier DP, Marshall CH, Entin JK, Pan M, Shi W, Koren V, Meng J, Ramsay BH, Bailey AA (2004) The multi-institution North American Land Data Assimilation System (NLDAS): utilizing multiple GCIP products and partners in a continental distributed hydrological modeling system. *Journal of Geophysical Research* **109**, D07S90.

Penman HL (1948) Natural evaporation from open water, bare soil, and grass. *Proceedings of the Royal Society A: Mathematical, physical and engineering sciences* **193**, 120–145.

Pinker RT, Tarpley JD, Laszlo I, Mitchell KE, Houser PR, Wood EF, Schaake JC, Robock A, Lohmann D, Cosgrove BA (2003) Surface radiation budgets in support of the GEWEX Continental-Scale International Project (GCIP) and the GEWEX Americas Prediction Project (GAPP), including the North American Land Data Assimilation System (NLDAS) project. *Journal of Geophysical Research: Atmospheres* **108**, D22.

Roy DP, Boschetti L, Justice CO, Ju J (2008) The Collection 5 MODIS Burned Area Product - Global evaluation by comparison with the MODIS Active Fire Product. *Remote Sensing of Environment* **112**, 3690–3707.

Xia Y, Mitchell K, Ek MB, Sheffield J, Cosgrove BA, Wood E, Luo L, Alonge C, Wei H, Meng J, Linvneh B, Lettenmaier DP, Koren V, Duan Q, Mo K, Fan Y, Mocko D (2012) Continental-scale water and energy flux analysis and validation for the North American Land Data Assimilation System project phase 2 (NLDAS-2): 1. Intercomparison and application of model products. *Journal of Geophysical Research* **117**, D03109.